NJC

Accepted Manuscript

This is an *Accepted Manuscript*, which has been through the Royal Society of Chemistry peer review process and has been accepted for publication.

Accepted Manuscripts are published online shortly after acceptance, before technical editing, formatting and proof reading. Using this free service, authors can make their results available to the community, in citable form, before we publish the edited article. We will replace this *Accepted Manuscript* with the edited and formatted *Advance Article* as soon as it is available.

You can find more information about *Accepted Manuscripts* in the Information for Authors.

Please note that technical editing may introduce minor changes to the text and/or graphics, which may alter content. The journal's standard Terms & Conditions and the Ethical guidelines still apply. In no event shall the Royal Society of Chemistry be held responsible for any errors or omissions in this *Accepted Manuscript* or any consequences arising from the use of any information it contains.

ROYAL SOCIETY OF CHEMISTRY

www.rsc.org/njc

New pyrazolyl dithioate function in the precursor for the shape controlled growth of CdS nanocrystals: optical, photocatalytic activities

Gopinath Mondal[a], Moumita Acharjya[a], Ananyakumari Santra[a], Pradip Bera[a], Sumanta Jana[b], Nimai Chand Pramanik[c], Anup Mondal[b] and Pulakesh Bera[a]*

[a]*Post Graduate Department of Chemistry, Panskura Banamali College, Vidyasagar University, Midnapore (E), West Bengal-721152, India*

[b]*Department of Chemistry, Indian Institute of Engineering Science and Technology (IIEST),Shibpur, West Bengal-711103, India*

[c]*Aerogel Laboratory, Centre for Materials for Electronics Technology (C-MET), Athani, M G Kavu PO, Thrissur 680581, India*

Abstract

The dithiocarbazate functionalized 3,5-dimethyl pyrazole ligands and their cadmium(II) complexes e.g., $[Cd(mdpa)_2Cl_2]$ (where mdpa is methyl ester of 3,5-dimethyl pyrazole-1-dithioic acid) and $[Cd(bdpa)_2Cl_2]$ (where bdpa is benzyl ester of 3,5-dimethyl pyrazole-1-dithioic acid) have been synthesized. The complexes are used as single-source precursors (SP) for the synthesis of spherical and rod likes CdS nanocrystals in a solvothermal process without using any external surfactants. *In situ* generated thiols (CH_3SH in case of mdpa complex and $PhCH_2SH$ in case of bdpa complex) in thermolysis of the SP govern the growth of nanocrystals. The spherical and rod shape CdS nanocrystals are produced in presence of CH_3SH and $PhCH_2SH$, respectively. A possible growth mechanism of nanocrystals based on the preferential thiol bonding to the nucleus is discussed. The nanocrystals were characterized by X-ray diffraction (XRD), transmission electron microscopy (TEM), and high resolution transmission electron microscopy (HRTEM) and X-ray photo electron spectroscopy (XPS). The UV-Vis spectroscopic studies of CdS nanocrystals show the quantum confinement effect with band gap 2.2 eV to 2.6 eV and the narrow intense PL emissions of the samples are red shifted (λ_{max}=570 nm) due to trap-related electron-hole recombination. The CdS nanocrystals

are successfully applied in the photodegradation of rose bengal (RB) and methylene blue (MB) dyes under visible light.

1. Introduction

Nanostructured metal sulphides have been extensively studied due to their importance in interpreting quantum size effect[1] and applications in a variety of devices such as solar cells[2–4] light-emitting diodes,[5] sensors,[6,7] lithium-ion batteries[8] and fuel cells.[1,7] Additionally, many metal sulphide semiconductor materials have been used as sensitizer for photo induced redox conversion of many organic pollutants, organic dyes to form eco-friendly end products.[9,10] Metal sulphides are a major group of materials that provide to the crystal chemists a high throughput due to their diverse dimensionality in structure.[11] In this context, CdS is one of the important n-type semiconducting materials belonging to group II-VI showing different physical, chemical and optical properties with respect to the corresponding "bulk" material.[12]

Various chemical methods have been used to synthesize CdS nanocrystals including solid state reactions,[13] self-propagating high temperature synthesis,[14] pyrolysis of single-source metal-organic precursors,[15–21] solvothermal syntheses,[22,23] microwave techniques,[24] ultrasonic irradiation,[25] hot injection method,[26] and so on. In these processes, surfactant like trioctyl phosphine (TOP), trioctyl phosphine oxide (TOPO), cetyl trimethyl ammonium bromide (CTAB), hexadecyl amine (HDA), hexaphosphonic acid (HPA) etc. were used which are highly toxic and have toxic effect on environment. So it remains an intriguing and ongoing challenge to exploit reliable, reproducible, robust, eco-friendly and facile methods for the synthesis of high quality CdS nanocrystals. In that respect, surfactant less solvothermal route using single-source precursors is one of the best green synthetic methods for preparation of CdS nanocrystals. Controlling the shape and size tuning of the nanocrystals can be achieved by tailoring the reaction parameters like concentration of the

SP, reaction time, temperature, solvent types and use of surfactants in different concentration. But the single-source route often embodied with demerits like broad size distribution and polydispersity of nanocrystals. However, few single-source precursors have been developed to produce nanocrystals of reasonable monodispersity which certainly provided the clear distinction of nucleation and growth process. Recent studies have shown that the shape and size of nanocrystals highly depended on rate of nucleation and monomer concentration at any instant along with other parameters like reaction time and temperature.[27] The solvent type used has also great influence in deciding the particle morphology. Very recently, it was showed that the precursor itself acts as preformed nuclei capable of structural rearrangement enabling the separation of nucleation and growth processes.[28–30] Thus size tuning is possible only by modifying the organic chromophores of the ligand in SP. However, the SP-directing shape controlled synthesis of nanocrystals is practically rare. Our present work uses two new pyrazolyl dithioate functionalized SP in the shape controlled synthesis of CdS nanocrystals. Thermolysis of SP furnished the products whose shape varies with the functional group present in the pyrazolyl dithiocarbazate precursor.

Dithiocarbamates (SS donor) and dithiocarbazates (NS donor) are special class of compounds with similar backbone[31] which can easily form metal complexes of low decomposition temperature. These low-melting complexes are exclusively used as single-source molecular precursors for the synthesis of MS nanoparticles.[17] Many dithiocarbamates metal complexes have been successfully used earlier in preparation of metal sulphide nanoparticles.[15–20] Other S-containing organic molecules such as thiosemicarbazide,[32] xanthates,[27] biurate[15,20] and thiourea[28] have also been used in the preparation of MS nanocrystals with different shape, size and crystallinity. Very recently designing of ligands for the synthesis of metal-organic precursor have been popularized for the facile synthesis of

good quality nanocrystals. Revaprasadu *et al*. used heterocycle based dithiocarbamates e.g., Cd(II)-piperidine dithiocarbamate and Cd(II)- tetrahydroisoquinoline dithiocarbamates as precursor for the synthesis of HDA and TOPO capped CdS nanorods, bipods and tripods.[20] N,N′-dioctyl/dicyclohexyl/diisopropyl/tetraethylenethiourea and dithiourea cadmium complexes are used as single precursor for the solvothermal synthesis of CdS nanocrystals.[28] Our group used the various main group metal complexes of dithiocarbazates to synthesize the different metal sulphide nanocrystals.[33–38] To obtain anisotropic nanocrystals, a kind of structure directing agent is needed.[28] The structure directing agents are generally the surfactants or the solvents used in the thermolysis. Scholes et al used the cadmium(II)-complexes of thiosemicarbazide and selenosemicarbazide that uniquely yield rod-shaped CdS and CdSe nanocrystals respectively without the aid of any external shape-directing agent.[28] The metal-organic single-source precursors itself dictate the growth direction of the nanocrystals. We reported earlier the preparation of CdS nanocrystals (spheres and rods) thermolysing Cd(II)-complex of S-benzyl dithiocarbazate in chelating solvents like hexamethylenediamine, ethylene glycol, ethylene diamine, hydrazine hydrate.[34] Rod shaped CdS particles are obtained in a solvothermal process using Cd-dithiocarbazate complex in hexamethylenediamine solvent.[33] It is assumed that the long chain diamine acts as structure-directing agent for anisotrpic growth of nanocrystals. But still the mechanism of shape evolution is unclear. To look inside the structure of SP on evolution of isotropic nanocrystal, we synthesized two functionalized pyrazolyl dithiocarbazate as building block of two new precursors *viz.* $[Cd(mdpa)_2Cl_2]$ and $[Cd(bdpa)_2Cl_2]$, and used them in shape controlled synthesis of nanocrystalline CdS spheres and rods, respectively in solvothermal process. CdS is one of the important n-type semiconducting materials belonging to group II-VI and used as catalyst for advanced photooxidation of organic pollutants owing to its appropriate band

potential for redox reaction. The prepared CdS shows excellent photocatalytic activity in photodegradation of organic dyes (RB and MB) under visible light irradiation.

2.Experimental Section

2.1 Chemicals

Cadmium chloride (Merck), carbon disulfide (Merck), acetyl acetone (Merck), methyl iodide (Spectrochem), benzyl chloride (Merck), ethylene diamine (Himedia), ethylene glycol (Himedia), N, N-dimethyl sulphoxide (Merck) were all of analytical grade and used without further purification. Solvent ethanol (Changshu Yangyuan Chemical, China) was dried and distilled before use.

2.2 Synthesis of ligands mdpa and bdpa:

2.2.1 Methyl-3,5-dimethyl pyrazole-1-carbodithioc acid (mdpa)

The ligand, methyl ester of 3,5-dimethyl pyrazole-1-carbodithioic acid (mdpa) was prepared in a reaction of 3,5-dimethylpyrazole (0.97 g, 10.0 mmol) in tetrahydrofuran (15 mL) with carbon disulfide (0.99 g, 13 mmol) and methyl iodide (1 mmol, 2.12 g) in an ice bath temperature with constant stirring.[38] The stirring was continuing for additional 1 hour where a yellow coloured compound of methyl ester of 3,5-dimethyl pyrazole-1-carbodithioc acid (mdpa) was separated out, filter off, washed with water and dried over silica gel. Yield: 82%. M.P. (decomposed): 30 °C. Anal. Calc. for $C_7H_{10}N_2S_2$: C, 45.13; H, 5.41; N, 15.04; S, 34.42. Observed: C, 45.01; H, 5.72; N, 15.48; S, 33.88. IR (cm^{-1}): 3398–3476, υ(O–H); 863, υ(C=S); 1585, υ(C=N); 1490, υ(C–N).

2.2.2 Benzyl-3,5-dimethyl pyrazole-1-carbodithioc acid (bdpa)

Benzyl 3,5-dimethylpyrazole-1-carbodithioic acid (bdpa) was prepared by the condensation of acetyl acetone (10 mmol, 1 mL) and S-benzyl dithiocarbazate (10 mmol, 1.9 g)[33,34] in 20

mL dry ethanol followed by addition of 5 mL glacial acetic acid. The cooled light yellow product was filtered off and washed with dry ethanol. M. P. 86 °C. Anal. Calc. for $C_{13}H_{14}N_2S_2$: C, 59.51; H, 5.38; N, 10.68; S, 24.44. Observed: C, 59.5; H, 5.40; N, 10.70; S, 24.50. IR (cm^{-1}): 3270, υ(O–H); 1572, υ(C=N); 1422, υ(C=C); 1020, υ(N=N);789, υ(C=S).

2.3 Synthesis of SP complexes $[Cd(mdpa)_2]Cl_2$ and $[Cd(bdpa)_2]Cl_2$

For the preparation of SP, 2.00 g of $CdCl_2.H_2O$ (10 mmol) dissolved in 20 mL dry ethanol was added to the ligand solution (20 mmol in 20 mL dry ethanol) with constant stirring for 10 minutes. Then the resulting mixture was refluxed in water bath temperature for 2 hours where upon a light yellow precipitation was obtained. The precipitation was then filtered off, washed with ethanol and dried in vacuum over silica gel. For $[Cd(mdpa)_2Cl_2]$: Yield 90%, MP (decomposition temperature) 145 °C, Λ_m=15 $\Omega^{-1}cm^2$ $mole^{-1}$, IR (cm^{-1}) 1571, υ(C=N); 789, υ(C=S) and for $[Cd(bdpa)_2Cl_2]$: Yield 82%, MP (decomposition temperature) 178 °C, Λ_m=18 $\Omega^{-1}cm^2$ $mole^{-1}$, IR (cm^{-1}) 1586, υ(C=N); 774, υ(C=S).

2.4 Synthesis of CdS nanocrystals

0.50 mmol of precursor was taken with 15 mL of ethylenediamine in a 50 mL two-necked round bottom flask placed with a condenser and thermocouple adaptor. The flask was degassed at room temperature for 5 minutes and then filled with inert nitrogen gas. The resulting solution was then gradually heated to 150 °C and maintained the reaction temperature for 30 minutes. Immediate after the reaction was stopped by adding cold ethanol.

Table–1: Reaction conditions and analytical results

$[Cd(mdpa)_2]Cl_2$					**$[Cd(bdpa)_2]Cl_2$**				
Solvent (mL)	Temperature in °C	Time (min)	Shape	Size (nm)	Solvent (mL)	Temperature in °C	Time min	Shape	Size (in nm)
EN (15)	150	30	spherical	8	EN (15)	150	30	rod shape	$80^a/10^b$
EG (15)	180	60	spherical	10	EG (15)	180	60	rod shape	$136^a/10^b$

DMSO (15)	200	90	spherical	12	DMSO (15)	200	90	rod shape	140[a]/10[b]

[a]*Average length*; [b]*Average diameter*

The yellow suspension was collected through centrifugation and washed 4 to 5 times with cold and dry ethanol. The same set of experiments was also done in EN at 180 °C for 1 hour with SP. The nanoparticle synthesis at 200 °C was done in DMSO. Dry powder of CdS nanocrystals were dried at 120 °C for 1 hour in vacuum oven. The reaction parameters and shape of the nanocrystals are given in Table−1.

2.5 Characterization

The elemental analysis (C, H, N, and S) of the complex was performed using FISONS EA-1108 CHN analyzer. The FTIR spectra (4000 cm^{-1}–500 cm^{-1}) were recorded on a Perkin Elmer Spectrum Two spectrophotometer. The samples were prepared using KBr pellets technique. The molar conductance values of the complexes were measured in a ethanolic solution with a systronics model 304 digital conductivity meter. The thermogravimetry analysis of precursor was carried out on Perkin Elmer TGA 4000 instrument at a heating rate 10 C/min under nitrogen. UV-Visible absorption spectra were recorded on a Perkin Elmer Lambda 35 spectrophotometer in 200–800 nm wavelength range at room temperature and photoluminescence (PL) spectra were recorded on F-7000 FL spectrophotometer. The photo catalytic activity was observed under 250W electric lamp. Powder X-ray diffraction (XRD) of the NCs was recorded using a Seifert XDAL 3000 diffractometer using graphite-monochromated Cu-Kα radiation (λ = 1.5418 Å) with a scan rate 5°/min over a range of $5° < 2\theta < 80°$ with steps of 0.02° and scintillation detector is operating at 40 kV and 40 mA. TEM and HRTEM of cadmium sulfide nanocrystals were characterized using a JEOL JEM–2100F EMI7220019 at an accelerating voltage 200 kV. The TEM samples were prepared by placing a drop of a dilute ethanol dispersion of nanocrystals on the surface of a 200-mesh carbon-coated copper grid. EDAX spectra were recorded on JEOL JSM-5800 Scanning

Microscope, OXFORD ISIS-300 microanalytical system. XPS was performed on a AXIS NOVA X-ray photoelectron spectroscopy, using monochromatic Al-Kα radiation with an anode voltage of 15 kV and emission current of 10 mA, the low resolution survey spectrum was recorded with a pass energy of 160 eV, high resolution spectrum was recorded with a pass energy of 20 eV, and the quantification was calculated by peak area measurement. Photocatalytic activity of CdS nanoparticles was studied with a 50 mL of 2.1×10^{-5} M and 1.7×10^{-5} aqueous solution of RB and MB, respectively in a 100 mL beaker using visible light source. A 250 W indoor fluorescent lamp was used as light source. The concentration of the dye after photocatalyst degradation was determined with a Perkin Elmer Lambda 35 UV-Vis spectrophotometer.

3. Result and discussion

3.1 Synthesis and characterization of SP

The condensation product of esters of dithioic acid viz. S-methyl dithiocarbazate (sdtc) and S-benzyl dithiocarbazates (bdtc) with acetyl acetone (acac) easily produces N^1 substituted 3,5-dimethyl pyrazole. In other word, the insertion of C(S)SR (carbodithioate) into the N–H bond of 3,5-dimethyl pyrazole makes the title ligands mdpa and bdpa. Pyrazole is considered to be the most flexible ligand in coordination chemistry due to its diatopic nature and the coordination flexibility of pyrazolido (pz-) ion.[39] The ease of synthesis of pyrazolyl ligands and their varieties of coordination modes with fascinating chemistry are the reasons for the study. The rich chemistry of pyrazole and their derivatives is attributed to the several chemical merits such as the presence of localized lone pair of electron on an in-plane orbital and the presence of low energy anti bonding vacant π* orbitals of the aromatic system guaranteed their π–acidity.[39] Keeping all in mind, we choose the functionalized pyrazolyl

ligands for the synthesis of functionalized SP so that it can play special properties in nanocrystals growth.

Solid state isolation and satisfactory results of the elemental analysis, conductance values and spectral studies reveals that the ligand and their cadmium complexes are of good purity and these are significantly stable in air. The ligands and their Cd(II)-complexes were characterized by means of elemental analyses, conductivity measurements, FTIR and Mass spectroscopy. The molar conductivities values of ~10^{-3} M solution in methanol prove the non-ionic nature of the cadmium complexes. The most probable composition of the cadmium complexes of mdpa and dbpa are $[Cd(mdpa)_2Cl_2]$ and $[Cd(bdpa)_2Cl_2]$, respectively based on conductance and FTIR results. The similar coordination behavior is also observed in the cadmium complex of dithiocarbamate.[40] FTIR spectra of the free ligands, cadmium complexes and the derived CdS nanoparticles from the Cd-complex precursor are shown in Fig.1. The very broad bands typical of water in the range of 3250–3470 cm^{-1} region in the IR spectra are the proof of hygroscopic nature of mdpa, bdpa and $[Cd(mdpa)_2Cl_2]$. A careful comparison of FTIR spectral data of the complexes with those of the ligands furnished considerable information regarding the mode of bonding of ligands. The peaks in the spectrum of complexes are less in number and quite sharp than the ligand's spectrum clearing proving the strong bonding of ligands with cadmium. Further redundancy of peaks in the spectrum of CdS nanoparticles (Curve c in Fig. 1A and 1B) clearly indicates the non-adherence of ligands in the surface of nanoparticles. The weak peaks appears in 1630 cm^{-1} for CdS derived from $[Cd(mdpa)_2Cl_2]$ (Curve c in Fig. 1A) or 1528 $cm^{-1}$for CdS derived from $[Cd(bdpa)_2Cl_2]$ (Curve c in Fig. 1B) may be due to the presence of trace amount of nitrogenous organic fragments in the samples. The presence of strong band at 1585 cm^{-1} for mdpa or at 1572 cm^{-1} for bdpa due to the $\upsilon_{C=N}$ (pyrazole ring) shifted to the higher frequency

by 12–25 cm^{-1} in their respective complex. These data indicate that the tertiary nitrogen atom of pyrazole ring was involved in bonding to Cd(II). The coordination of the thione sulphur

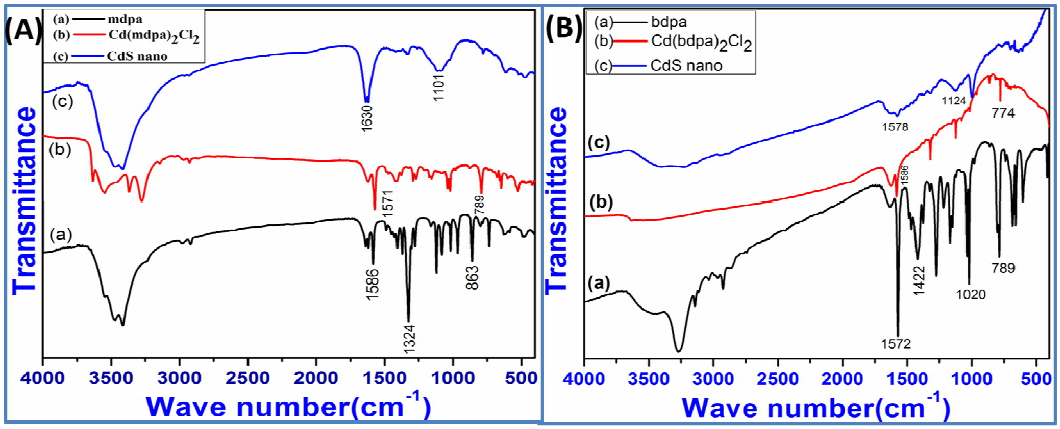

Figure-1: FTIR spectra: A [mdpa, $Cd(mdpa)_2Cl_2$ and CdS nanocrystals derived from $Cd(mdpa)_2Cl_2$] and B [bdpa, $Cd(bdpa)_2Cl_2$ and CdS nanocrystals derived from $Cd(bdpa)_2Cl_2$] from EG at 180°C.

atom to the cadmium is indicated by a decrease of the $\upsilon_{C=S}$ band from 860 cm^{-1} in mdpa or 861 cm^{-1} in bdpa to 792 cm^{-1} in $[Cd(mdpa)_2]Cl_2$ or 784 cm^{-1} in $[Cd(bdpa)_2Cl_2]$, respectively. The positive shifts of the $\upsilon_{N\text{-}Npz}$ frequencies 1292 cm^{-1} for mdpa or 1250 cm^{-1} in bdpa to *ca.* 30 cm^{-1} on complexation with Cd(II) indicated the involvement of pyrazolyl tertiary nitrogen in bonding. Similar results also found in the cadmium complexes of ligands with similar structural backbone.[40]

Thermogravimetry analysis is conducted to study the thermal behavior and suitability of the precursors for the preparation of CdS. The TGA curves of $[Cd(mdpa)_2Cl_2]$ and $[Cd(bdpa)_2Cl_2]$ are given in Figure 2. The three steps decomposition process of the precursor $[Cd(mdpa)_2Cl_2]$ starts at the temperature 120 °C and is completed by 750 °C. The first step decomposition (found mass loss 34.48%) is accompanied with the combined loss of one Cl and one ligand unit except one sulfur atom (*ca.* 34.08%) (see supplementary materials). The

second step of mass loss is attributed to the loss of SCH_3 unit (*ca.* 9.44%) giving a residue which is stable up to 550 °C. In the final step of decomposition (39.01%), the residual ligand

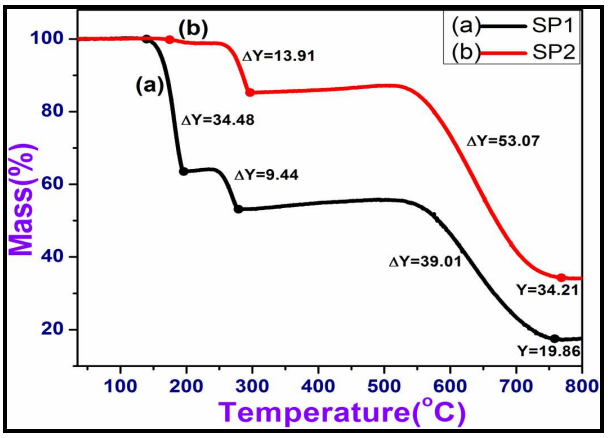

Figure-2: TG analysis of (a) $[Cd(mdpa)_2Cl_2]$ (SP1) and (b) $[Cd(bdpa)_2Cl_2]$ (SP2).

unit is lost to form CdS which again losses the surface trapped S at higher temperature to form finally the metallic Cd residue (*ca.* 20.21%). The decomposition of $[Cd(bdpa)_2Cl_2]$ started at 120 °C following two major decomposition steps. The first step is attributed to the loss of $–CH_2Ph$ unit (*ca.* 12.85 %) giving a residue that is stable up to *ca.* 550 °C. The major loss is occurred in the last step of decomposition which is attributed to the loss of all organics followed by reversible addition of gaseous sulfur atoms to the metallic cadmium giving a residue $[CdS]S_3$ (*ca.* 33.89%). The TGA curves of the precursors also serve a guideline in deciding the thermolysis temperature of the precursors. The thermolyses of the SPs were performed at 150°C, 180°C and 200°C to avoid any incomplete decomposition.

3.2 Morphology and characterization of CdS NPs:

X-ray diffraction (XRD) patterns for the nanocrystals synthesized at different temperature are shown in Fig.3. The diffraction patterns of the samples are indexed to wurtize (hexagonal) phase of CdS with characteristics (100), (002), (101), (102), (110), (103), and (112) peaks (JCPDS number 041–1049). The broad peak in the XRD patterns (Fig.3c) of sample

obtained from EG at lower growth temperature (150°C) reveals small size and amorphous nature of the sample whereas sharp peaks (Fig. 3a, 3b) for the samples at higher growth

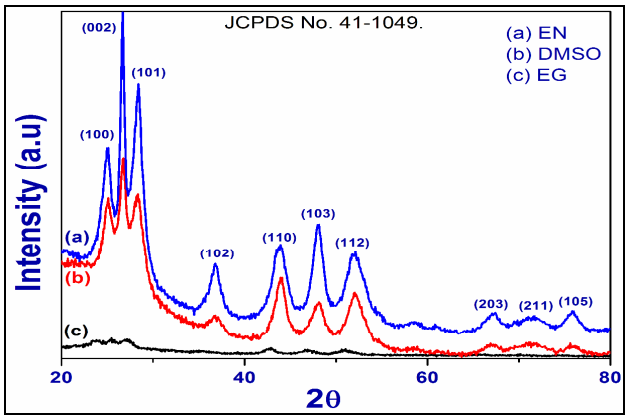

Figure-3: X-ray diffraction patterns of CdS nanocrystals prepared from $[Cd(bdpa)_2Cl_2]$ in EN (a), DMSO (b) and $[Cd(mdpa)_2Cl_2]$ in EG (c) at 180°C.

The morphology and microstructures of the as-synthesized CdS nanocrystals were characterized by TEM and SEM analyses. Fig. 4 shows TEM and high resolution TEM pictures of CdS nanocrystals prepared at different reaction conditions and the average particle sizes as calculated from TEM images are given in Table 1. Nearly spherical CdS particles can be seen in the high resolution TEM images (Fig.4A and 4B) of the samples prepared from $[Cd(mdpa)_2Cl_2]$ using EG and EN, respectively at 150^{o}C. The sizes of synthesised nanocrystals are found to be 8–10 nm at various reaction conditions. At higher reaction temperature e.g., 180 ^{o}C the product morphology is same but a very small increase of size observed. The SAED image of single spherical CdS nanocrystals prepared from $[Cd(mdpa)_2Cl_2]$, is indicative of clear crystallinity of the particles with all possible

diffractions of planes as shown in the Fig.4C. The measured lattice spacing for the CdS

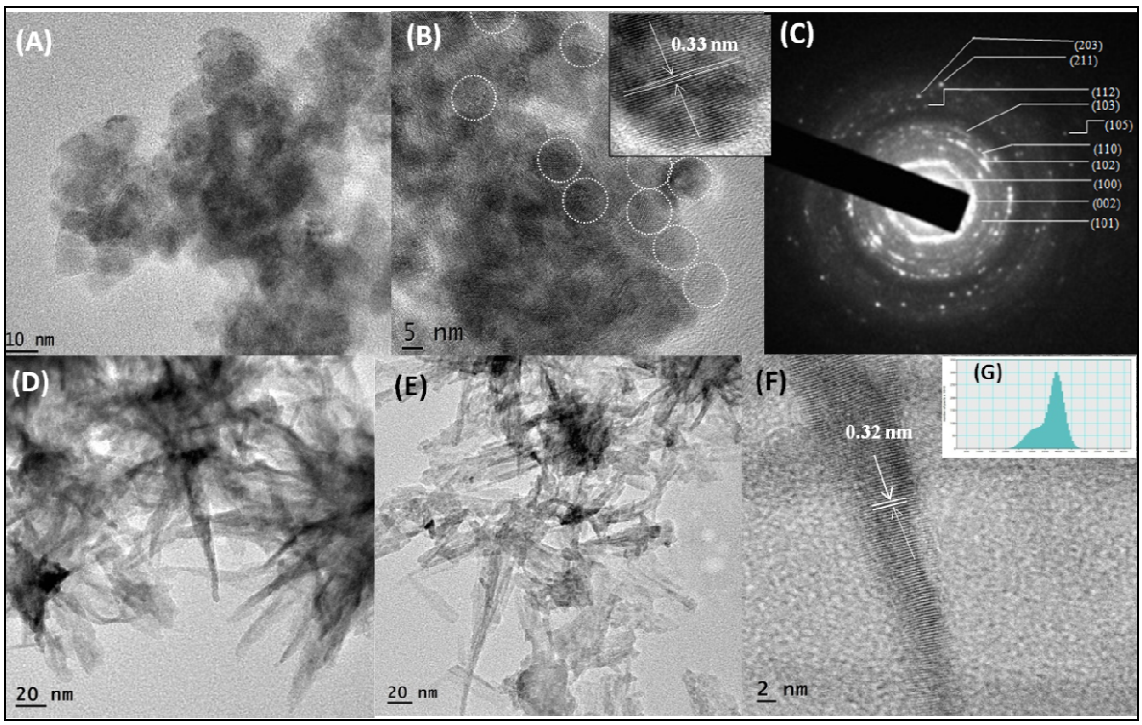

Figure-4: TEM/HRTEM images of CdS nanocrystals obtained from $[Cd(mdpa)_2Cl_2]$ in EG at 150°C (A), in EN at 180°C (B), and SAED image of CdS nanocrystals from $[Cd(mdpa)_2Cl_2]$ in EG at 150°C (C), TEM/HRTEM images of CdS nanocrystals obtained from $[Cd(bdpa)_2Cl_2]$ in EG at 180°C (D), in EN at 180°C (E & F), and histogram of the sample (G).

nanocrystals from EG at 180 ^oC is found 3.3 nm (inset of Fig. 4B) which corresponds the diffraction of (002) plane. It has been observed that SP functionalized with $–SCH_3$ group i.e., $[Cd(mdpa)_2Cl_2]$ results only spherical morphology irrespective to the solvent used in the thermolysis. The high resolution TEM images for the samples obtained from $–SCH_2Ph$ functionalized SP i.e., $[Cd(bdpa)_2Cl_2]$ in EG and EN at 180 ^oC are given in the Fig.4D and 4E, respectively. Urchin like CdS hierarchical nanostructure results irrespective of solvent used in the thermolysis of $[Cd(bdpa)_2Cl_2]$. The nanostructure is composed of many nanorods which self assembled into an urchin-like architecture. The average diameter of the nano rods higher at the centre of the structure than the open ended side by about 4 to 5 times indicating non-uniformity nature of the nano architectures. These kinds of coarse architecture are

capable of showing catalytic activity. The d-spacing observed (Fig.4F) corresponds to (002) plane of hexagonal CdS. The growth direction of these (002) facets are anisotropic, suggesting the retardation of large numbers of (110) facets in the nanostructures. In addition to determine proper crystallinity the energy-dispersive X-ray spectroscopy (EDX) analysis of CdS nanocrystals was done in carbon coated copper grid, which confirmed that the elemental composition of Cd:S≈1:1 and no precursor element remain after reaction (Fig.S1 and S2).

The XPS spectrum of the sample prepared from EN at 180°C, was done to check the atomic composition and surface chemistry. The Cd 3d spectrum has a doublet feature due to the spin orbit splitting resulting into $3d_{5/2}$ and $3d_{3/2}$ peaks with a spin orbit separation 7.0 eV. The doublet peaks that were assignable to Cd $3d_{5/2}$ and Cd $3d_{3/2}$, respectively were observed at 405.1 eV and 412.1 eV (Fig.5) in the CdS sample. Apart from cadmium 3d, other core levels of interest in the materials are S 2p and S 2s. The S 2p spectrum exhibits a doublet arising from the spin orbit splitting in the region 168.0 eV that can be assigned to the form Cd –S– and the additional shake up peak at 166 eV is attributed to the oxidized sulfur species. The S 2s spectrum has a single peak feature appearing at binding energy 225 eV with shake up features which is observed earlier.[41] The oxygen on the surface at 532 eV may be due to the presence of chemisorbed oxygen.

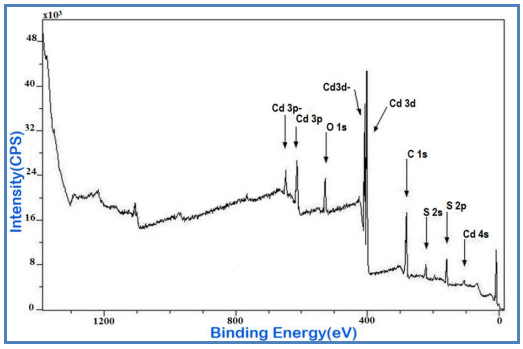

Figure-5: XPS spectrum of CdS nanocrystals prepared from $[Cd(mdpa)_2Cl_2]$ using EG at 180°C.

3.3 Optical properties of CdS nanoparticles

Fig.6 illustrates the UV-VIS absorption spectra of CdS nanocrystals dispersed in distilled ethanol at room temperature. The appearance of strong absorbance peak at 480 nm (Fig. 6a) of the sample obtained from $[Cd(mdpa)_2Cl_2]$ in EG (180°C) whereas the same characteristics bands are observed for the sample obtained from $[Cd(bdpa)_2Cl_2]$ at 480 nm and 485 nm (Fig. 6b and 6c) in EN (180°C) and DMSO (200°C). The band gap plots of $(\alpha h\upsilon)^2$ vs. E(=hυ) shows the band gaps between conduction to valence band appeared at 2.2 eV, 2.5 eV and 2.6 eV [inset of Fig. 6] indicates good solar energy absorbers. Figure 7 shows the PL emission spectra measured at room temperature for the CdS nanocrystals obtained from different single source precursors. The spectra exhibit a narrow peak at 480 nm corresponding to the band-edge emission along with another red shifted narrow intense peak in the region 570 nm. This red shifted emission results from the trap related electron-hole recombination. It is to be noted that the samples obtained from different precursor emit at the same λ_{max} position with different emission intensity and peak width. The CdS obtained from $[Cd(bdpa)_2Cl_2]$ shows a narrow and sharp emission peak with higher intensity (Fig. 7b) than the CdS obtained from $[Cd(mdpa)_2Cl_2]$ (Fig. 7a) which proves better electronic passivation of CdS surface by the $PhCH_2SH$ than CH_3SH. An emission peak in the region 500–700 nm is often observed for CdS nanocrystal which is attributed to recombination of trapped electron-hole in the surface defect states.[42,43] The trap state emission relates to the surface chemistry and structure of the CdS nanocrystals. The band edge and trap-state photoluminescence indicate that the CdS sample has a suitable band gap position for photocatalytic decomposition of organic dyes under visible light irradiation.

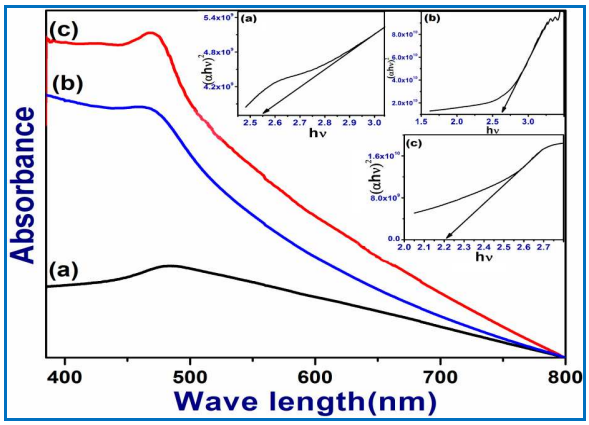

Figure-6: UV-Vis spectra and band gap value of CdS nanocrystals obtained from $[Cd(mdpa)_2Cl_2]$ using EG at 180°C (a), from $[Cd(bdpa)_2Cl_2]$ using EN (180°C) (b), and from $[Cd(bdpa)_2Cl_2]$ using DMSO (200°C) (c).

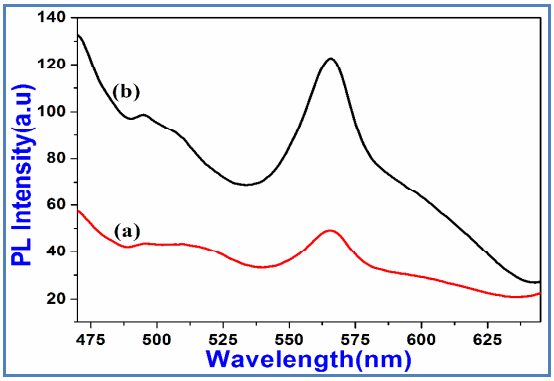

Figure-7: PL emission spectra of CdS nanocrystal obtained from $[Cd(mdpa)_2Cl_2]$ using EN at 150°C (a), from $[Cd(bdpa)_2Cl_2]$ using DMSO at 200°C (b).

3.4 Growth Mechanism of CdS nanocrystals

In SP method, Factors generally resulted that thermodynamic stable spherical products are the fast nucleation and the quick passivation of the seeded crystals in the presence of high concentration of stabilizing agent(s) at high reaction temperature. Most of the SPs those so far used in solvothermal method produced spherical particles. On the other hand, the anisotropic growth of nanocrystals depends on several factors like use of molecular template(s), use of copious capping agents and the lower activation energy of SP.[15–20] In case of dithiocarbamates and xanthates precursor, the M–S bond template useful for controlling

the shape of nanocrystals. Strous *et al.* proposed that the metal clusters act as preformed nuclei which on structural rearrangement without dissolution enabling to produce 1D nanostructures.[30] Vittal *et al.* reported the shape controlled synthesisi of Ag_2S nanoparticles using a 'nucleation initiator' e.g., hexadecyl amine (HDA) which helps to separate nucleation and growth. It was proposed that the coordinating solvent plays a crucial role in deciding particle morphology. CdSe nanorod formation is attributed to the higher coordinating nature of hexaphosphonic acid. Revaprasadu *et al.* reported the influence of solvent in controlled synthesis of CdS particles from the heterocyclic dithiocarbamate cadmium complex. Where spherical and elongated CdS nanoparticles were obtained from trioctyl phosphine oxide (TOPO) and hexadecyl amine (HDA) using the same heterocyclic precursor.

The effect of solvent is also reflected in our earlier reports of synthesis of spherical and rod–like particle from the same single-precursors i.e., cadmium complex of S-benzyl dithiocarbazate (sbdtc)[33,34] and/or copper complex of S-methyl dithiocarbazate (smdtc)[36,38] were performed by changing the solvent. We observed that use hexamethylene diamine (HMDA) and ethylene diamine (EN) solvent in the pyrolysis of $[Cd(sbdtc)_2Cl_2]_2$ selectively produces rod shape 1D-CdS nanocrystals. Whereas other bidentate ligands ethylene glycol (EG) and hydrazine hydrate (HH) produced only spherical product in the thermolysis of $[Cd(sbdtc)_2Cl_2]_2$.[34] Especially chelating diamines e.g., EN or HMDA where two nitrogen atoms are separated by more than two carbon centres could form stable intermediate chelate complexes with metal ion displacing ancillary ligands and there we proposed that the intermediate stable complex with coordinating solvent acts as molecular template for the synthesis of anisotrpic structure. Solvents other than chelating diamine could not able to form intermediate stable complexes as a consequence thermodynamically stable spherical nanocrystals are expected. It was also observed that when the coordination environment of SP is fairly stable with high level of coordination saturation, the primary SP structure was not

affected by any kind of chelating/coordinating solvent.[37] Octa-coordinated Pb-complex of sbdtc always furnished spherical nanoparticles irrespective of solvent used and the in situ generated organic fragment e.g., CH_3SH stabilized the seeded crystals. Besides solvent effect in crystal evolution, the special structural characteristics of SP is responsible for anisotropic growth as reflected in the recent works.[28,29] G.D. Scholes *et al.* proposed that Cd-complexes of thiosemicarbazide or seleno semicarbazide precursors with very low activation energy barrier (2.1 KJ/mol) were capable to produce rod-shape CdS where the little higher activation energy in the range 18.0 KJ/mol furnished spherical CdS.[28]

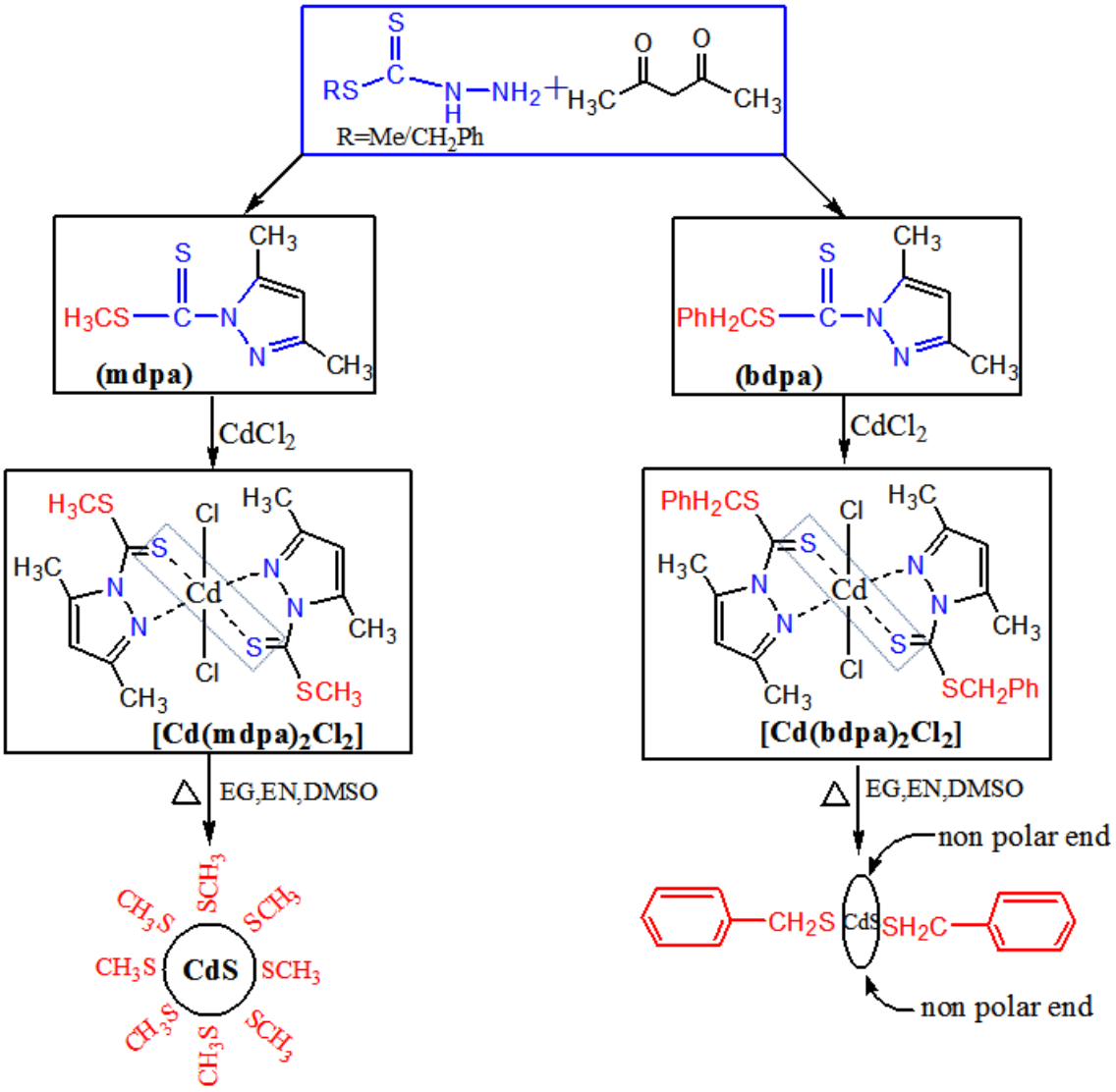

Scheme-1: Synthesis of SPs and formation mechanism of CdS nanoparticles

In the present work, the extra stability to the SP was confirmed by incorporating the heterocyclic pyrazole with thiolato environment. The smdtc and sbdtc were converted to mdpa and bdpa, respectively which provides stable environment to the cadmium centre so that the participating solvent in the thermolysis cannot displace them. In our method, the solvent used to serve the heat transferring medium. With the heat the molecular transformation takes place in the coordination environment of $[Cd(mdpa)_2Cl_2]$ or $[Cd(bdpa)_2Cl_2]$. The internal rearrangement of the metal centre which can be regarded as molecular template starts the nucleation and the growth of nanoparticles monitored by the fragmented thiol. In reaction condition, $[Cd(mdpa)_2Cl_2]$ provides small thiol ligand, CH_3SH and $[Cd(bdpa)_2Cl_2]$ provides relatively bulkier thiol, $PhCH_2SH$. Small thiol CH_3SH can bind strongly to all the facets of seed crystals giving only spherical nanoparticles where the bulkier thiol $PhCH_2SH$ preferentially binds the polar facets of nucleus giving an opportunity to grow the nanocrystals anisotropically. The proposed mechanistic pathways are summarized in the scheme 1. It is to be noted that the shape and size of the nanocrystals do not vary significantly with the concentration of the SP when other parameters were unaltered.

3.5 Photo catalytic activity of CdS NCs

The chores architecture and the trap states in the crystal surface of CdS samples as ascertained from TEM and PL spectra respectively might be good photo catalyst. Photon energy greater than the band gap energy of CdS produced electron-hole pair. Such photo generated electron (e^-) and hole (h^+) are subsequently transfer to the surface of the crystal. Subsequently, e^- and h^+ react with H_2O and molecular O_2 to generate $OH^{\bullet}$ and O^{2-}radicals. These radicals decompose the organic dyes following free radical oxidation and reduction processes. To investigate the potentiality of the synthesised CdS nanocrystals as photo-catalyst, the catalytic performances were examined by photo degradation of RB and MB

under a visible light illumination. We have chosen RB, MB like organic dyes to test the photocatalytic activity, since these are fluorescence dyes and commonly used in textile, photographic and photochemical industries. The synthesised semiconducting CdS nanocrystals have been used as catalyst for photodegradation under visible light. Fig. 8 shows the time dependent VU-VIS spectral change of RB and MB solution in the presence of CdS nanocrystals under the irradiation of light for 90 min and 65 min, respectively. Photocatalytic activity of CdS nanocrystals were studied with 50 mL aqueous solution of each 2.1×10^{-5} M RB and 1.7×10^{-5} M MB taken in a 100 mL beaker with 15 mg CdS under a 250W indoor fluorescent lamp as visible light source. The solutions were store in dark to attend adsorption desorption equilibrium for 40 min and then the solutions were exposed in visible light with magnetic stirring.

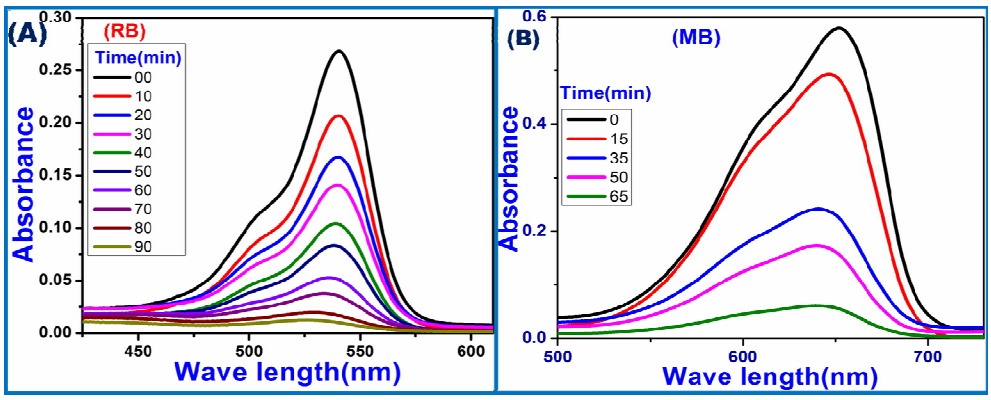

Figure-8: Time dependant spectral changes of aqueous RB (A) and MB (B) solution by CdS nanocrystals prepared from $[Cd(mdpa)_2Cl_2]$ and $[Cd(bdpa)_2Cl_2]$, respectively

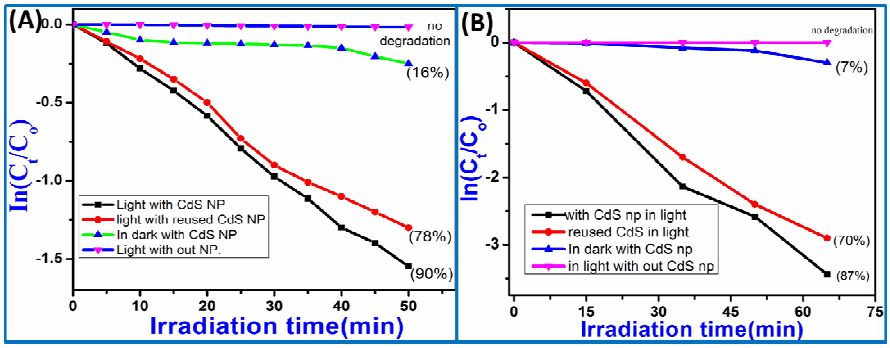

Figure-9: Logarithmic change in concentration of dyes as a function of irradiation time (A) for RB and (B) for MB

At a certain time interval 3mL of solution was centrifuged and measured adsorption in UV-Vis spectrophotometer. The characteristics absorption peaks appeared at 540 nm and 650 nm for RB and MB solution respectively and gradually decrease with irradiation time. After 90 min (for RB) and 65 min (for MB) reaction time no new absorption peaks appeared, but the characteristic absorption bands of the dyes disappeared which suggesting the complete photo degradation of RB and MB. In order to determine the kinetics of the photo degradation, we plot $\ln(C_t/C_o)$ with Irradiation time(t) (Fig. 9) in equation $\ln(C_o/C_t) = kt$, where C_o be the initial concentration of aqueous solution, C_t be the concentration at time t and k is rate constant for the reaction. The measured k values are 3.5×10^{-3} min $^{-1}$ and 4.8×10^{-3} min^{-1} for photo degradation in RB and MB, respectively. Degradation processes follows first order kinetics.

4. **Conclusion**

Functionalization with alkyl and aryl carbodithioate group in N^1 position of 3,5-dimethyl pyrazole make the chelates with soft sulphur and soft nitrogen donor atoms and form easily air-stable cadmium(II) complexes e.g., $[Cd(mdpa)_2Cl_2]$ and $[Cd(bdpa)_2Cl_2]$. TGA analyses of the complexes reveal their low decomposition temperature and suitability to act as single-source precursor for CdS nanocrystals. The single-source precursors are used in shape controlled synthesis of hexagonal CdS nanocrystal in solvothermal process without using

external surfactants. The SP, $[Cd(mdpa)_2Cl_2]$ with SCH_3 group in the structure always produced spherical CdS nanoparticles where SP, $[Cd(bdpa)_2Cl_2]$ with SCH_2Ph group selectively furnished rod-liked CdS nanoparticles in the solvothermal reaction irrespective of solvent. We conclude that the evolution of spherical or rod shaped nanocrystals depends on the substituent(s) present in the precursor irrespective the solvent used in the thermolysis. Different reaction temperatures and nature of solvent have no profound effects on the shape other than increase of the particle sizes. It is proposed that the methane thiol (CH_3SH) in case of $[Cd(mdpa)_2Cl_2]$ or benzyl thiol ($PhCH_2SH$) in case of $[Cd(bdpa)_2Cl_2]$ produced in the reaction conditions and act as structure directing agent as well as stabilizing agent. Being a smaller thiol, CH_3SH can effectively binds all the facets of seeded crystals facilitating isotropic growth whereas bulky $PhCH_2SH$ binds selective polar facets forming rod shaped structures. The average sizes of the spherical nanocrystals are found to 8 to 12 nm as evidenced by TEM analysis. The nanocrystals show quantum confinement effect with band gap ~2.2 eV. The PL emissions of the samples are red shifted and are trap-related. The CdS nanocrystals have shown to be excellent catalyst in photo degradation of aqueous solution of Rose Bengal and Methylene Blue under visible light irradiation. We can predict that only heating effect can cause solid state transformation of single molecular precursor to controlled shape of nanocryatals. Further exploration is needed for beter understanding of the structure-activity of precursor and nanoproducts with respect to shape, size and crystallinity.

Acknowledgements

We gratefully acknowledge to CSIR, Government of India [grant no. 1(2534)/11/EMR-II], and UGC, Government of India [F 42-280/2013(SR)] for financial support. The authors thank to Professor Sang Il Seok, Department of Energy Science, Sungkyunkwan University, Suwon 440-746, South Korea for XPS analysis. We are thankful to Professor Dipankar Chattopadhyay of Centre for Research in Nanoscience & Nanotechnology (CRNN),

University of Calcutta, JD-2, Salt Lake City, Kolkata 700098, West Bengal, India for TEM analyses.

References:

1. M. R Gao, Y. F Xu, J. Jiang and S. H. Yu, *Chem. Soc. Rev.,* 2013, **42**, 2986-3017.

2. F. Cao, H. Wang, Z. Xia, X. Dai, S. Cong, C. Dong, B. Sun, Y. Lou, Y. Sun, J. Z and G. Zou, *Materials Chemistry and Physics,* 2015, *149-150*, 124–128.

3. K. Yuan, L. Chen, L. Tan and Y. Chen, Chemistry-A European Journal, 2014 20 (10.1002/chem.v20.20), 6010-6018

4. J. Albero, J. N. Clifford and E. Palomares, *Coordination Chemistry Reviews***,** 2014**, 263–264,** 53–64.

5. Y. L. Kong, I. A. Tamargo, H. Kim, B. N. Johnson, M. K. Gupta, T-W. Koh, H-A. Chin, D. A. Steingart, B. P. Rand and M. C. McAlpine, *Nano Lett.*, 2014, **14(12)**, 7017–7023.

6. J. Liu, D. Xue, *J. Mater. Chem.,* 2011, **21**, 223–228.

7. C. H. Lai, M. Y. Lu, L. J Chen, *J. Mater. Chem.,* 2012, **22**, 19–30.

8. K. Chang and W. Chen**,** *Chem. Commun.***,** 2011, **47**, 4252–4254.

9. W. T. Yao, S. H. Yu, S. J. Liu, J. P. Chen, X. M. Liu and F. Q. Li, *J. Phys. Chem. B,* 2006, **110(24),** 11704–11710.

10. A. K. Sahoo and S. K. Srivastava, *J Nanopart Res.,* 2013, **15,** 1591–1606.

11. S. Shen and Q. Wang, *Chem. Mater.,* 2013, **25(8)**, 1166–1178.

12. D. Fan, M. Afzaal, M. A. Mallik, C. Q. Nguyen, P. O'Brien and P. J. Thomas, *Coordination Chemistry Reviews,* 2007, **251(**13–14), 1878–1888.

13. W. Wang, Z. Liu, C. Zheng, C. Xu, Y. Liu, G. Wang, *Materials Letters,* 2003, 2755–2760.

14. A. Makino, *Progress in Energy and Combustion Science*, 2001, **27**, 1–74.

15. K. Ramasamy, M. A. Malik, M. Helliwell, J. Raftery, and Paul O'Brien, *Chem. Mater.*, 2011, **23(6),** 1471–1481.

16. M. A. Malik, N. Revaprasadu and Paul O'Brien, *Chem. Mater.*, 2001, **13(3)**, 913–920.

17. M. A. Malik**,** M. Afzaal and P. O'Brien, *Chemical Reviews***,** 2010, **110(7)**, 4417–4446.

18. L. D. Nyamen, N. Revaprasadu, R. V.S.R. Pullabhotla, A. A. Nejo, P. T. Ndifon, M. A. Malik and P. O'Brien, *Polyhedron,* 2013**, 56**, 62–70.

19. N. Srinivasan, S. Thirumaran and S. Ciattini, *Journal of Molecular Structure,* 2012, **1026**, 102–107.

20. L. D. Nyamen, V. S. R. Pullabhotla, A. A. Nejo, P. Ndifon and N. Revaprasadu, *New J. Chem.***,** 2011, **35**, 1133–1139.

21. A. L. Abdelhady, M. A. Malik and Paul O'Brien, *J. Inorg Organomet Polym,* 2014, **24**, 226–240.

22. D. Xu , Z. Liu , J. Liang and Yitai Qian, *J. Phys. Chem. B*, 2005, **109 (30)**, 14344–14349.

23. J. Park, J. Joo, S. G. Kwon, Y. Jang and T. Hyeon, *Angew. Chem. Int. Ed.*, 2007, **46**, 4630–4660.

24. Y. Wada, H. Kuramoto, J. Anand, T. Kitamura, T. Sakata, H. Mori and S. Yanagida, *J. Mater. Chem.***,** 2001, **11**, 1936–1940.

25. N. Ghows and M. H. Entezari, *Ultrasonics Sonochemistry*, 2011, **18,** 269–275.

26. C. B. Murray, C. J. Norris and M. G. Bawendi, *J. Am. Chem. Soc.,* 1993, **115**, 8706–8715.

27. N. Pradhan, B. Katz and S. Efrima, *J. Phys. Chem. B*, 2003, **107 (50)**, 13843–13854.

28. P. S. Nair and G. D. Scholes, *J. Mater. Chem.***,** 2006, **16**, 467–473.

29. T. Mondal, G. Piburn, V. Stavila, I. Rusakova, T. O. Ely, A. C. Colson and K. H. Whitmire, *Chem. Mater.,* 2011, **23,** 4158–4163.

30. S. L. Cumberland, K. M. Hanif, A. Javuer, G. A. Khitrov, G. F. Strouse, S. M. Woessner and C. S. Yun, *Chem. Mater.,* 2002, **14**, 1576–1584.

31. M.A. Ali, A.H. Mirza, M.H.S.A. Hamid, P.V. Bernhardt, O. Atchade, X. Song, G. Eng, L. May, *Polyhedron,* 2008*,* **27**, 977–984.

32. P. S. Nair, T. Radhakrishnan, N. Revaprasadu, G. A. Kolawole and P. O'Brien, *Chem. Commun.,* 2002, **6**, 564–565.

33. P. Bera, C. H. Kim and S. I. Seok, *Solid State Sciences*, 2010, **12**, 532–535.

34. P. Bera, C. H. Kim and S. I. Seok. *Solid State Sciences,* 2010, **12**, 1741–1747.

35. P. Bera and S. I. Seok, *J Nanopart Res.,* 2011, **13**, 1889–1896.

36. P. Bera and S. I. Seok, *Solid State Sciences,* 2012, **14,** 1126–1132.

37. G. Mondal, A. Santra, S. I. Seok and P. Bera, *J. Nanosci. Lett.,* 2014, **4,** 35.

38. G. Mondal, P. Bera, A. Santra, S. Jana, T. N. Mandal, A. Mondal, S. I. Seok and P. Bera, *New J. Chem.,* 2014, **38**, 4774–4782.

39. J. Perez and L. Liera, *Eur. J. Inorg. Chem.,* 2009, 4913–4925.

40. P. Bera, C. H. Kim and S. I. Seok, *Polyhedron*, 2008, **27**, 3433–3438.

41. M. Stoev and A. Katerski, *J. Mater. Chem.***,** 1996, **6**, 377–380.

42. A. E. Saunders, A. Ghazelbash, P. Sood and B. A. Korgel, *Langmuir,* 2008, **24**, 9043–9049.

43. S.F. Wuiester, C. M. Donega and A.Meijerink, *J. Phys.Chem. B.,* 2004, **108**, 17393.

Table-1: Reaction parameters and shape of the nanocrystals.

Scheme-1: Synthesis of SPs and formation mechanism of CdS nanoparticles.

Figure-1: FTIR spectra: A [mdpa, $Cd(mdpa)_2Cl_2$ and CdS nanocrystals derived from $Cd(mdpa)_2Cl_2$] and B [bdpa, $Cd(bdpa)_2Cl_2$ and CdS nanocrystals derived from $Cd(bdpa)_2Cl_2$] from EG at 180°C.

Figure-2: TG analysis of (a) $[Cd(mdpa)_2Cl_2]$ (SP1) and (b) $[Cd(bdpa)_2Cl_2]$ (SP2).

Figure-3: X-ray diffraction patterns of CdS nanocrystals prepared from $[Cd(bdpa)_2Cl_2]$ in EN (a), DMSO (b) and $[Cd(mdpa)_2Cl_2]$ in EG (c) at 180°C.

Figure-4: TEM/HRTEM images of CdS nanocrystals obtained from $[Cd(mdpa)_2Cl_2]$ in EG at 150°C (A), in EN at 180°C (B), and SAED image of CdS nanocrystals from $[Cd(mdpa)_2Cl_2]$ in EG at 150°C (C), TEM/HRTEM images of CdS nanocrystals obtained from $[Cd(bdpa)_2Cl_2]$ in EG at 180°C (D), in EN at 180°C (E & F), and histogram of the sample (G).

Figure-5: XPS spectrum of CdS nanocrystals prepared from $[Cd(mdpa)_2Cl_2]$ using EG at 180°C.

Figure-6: UV-Vis spectra and band gap value of CdS nanocrystals obtained from $[Cd(mdpa)_2Cl_2]$ using EG at 180°C (a), from $[Cd(bdpa)_2Cl_2]$ using EN (180°C) (b), and from $[Cd(bdpa)_2Cl_2]$ using DMSO (200°C) (c).

Figure-7: PL emission spectra of CdS nanocrystal obtained from $[Cd(mdpa)_2Cl_2]$ using EN at 150°C (a), from $[Cd(bdpa)_2Cl_2]$ using DMSO (200°C) (b).

Figure-8: Time dependant spectral changes of aqueous RB (A) and MB (B) solution by CdS nanocrystals prepared from $[Cd(mdpa)_2Cl_2]$ and $[Cd(bdpa)_2Cl_2]$, respectively.

Figure-9: Logarithmic change in concentration of dyes as a function of irradiation time (A) for RB and (B) for MB.

TOC

New pyrazolyl dithioate function in the precursor for the shape controlled growth of CdS nanocrystals: optical, photocatalytic activities

Gopinath Mondal, Moumita Acharjya, Ananyakumari Santra, Pradip Bera, Sumanta Jana, Nimai Chand Pramanik, Anup Mondal and Pulakesh Bera*